Development of a secondary triton beam from primary ^{16,18}O beams for (t,^{3}He) experiments at intermediate energies. [1]

G.W. Hitt [a,b,c] Sam. M. Austin [a,c] D. Bazin [a] A.L. Cole [a,c,2]

J. Dietrich [d] A. Gade [a,b] M.E. Howard [e] S.D. Reitzner [e,3]

B. M. Sherrill [a,b,c] C. Simenel [a,f] E.E. Smith [e] J. Stetson [a]

A. Stolz [a] R.G.T. Zegers [a,b,c,*]

[a] *National Superconducting Cyclotron Laboratory, Michigan State University, East Lansing, MI 48824-1321, USA*

[b] *Department of Physics and Astronomy, Michigan State University, East Lansing, MI 48824, USA*

[c] *Joint Institute for Nuclear Astrophysics, Michigan State University, East Lansing, MI 48824, USA*

[d] *Department of Physics, Technische Universität Dresden, Dresden D-01062, Germany*

[e] *Department of Physics, The Ohio State University, Columbus, OH 43210, USA*

[f] *DSM/DAPNIA CEA Saclay, F-91191 Gif-sur-Yvette, France*

Abstract

A new method to produce a secondary beam of tritons (^{3}H) at intermediate energies ($E_t > 100$ MeV/nucleon) has been developed. The triton beam intensities for primary ^{16,18}O beams of 150 and 120 MeV/nucleon, respectively, were studied. The best results are obtained with a ^{16}O beam of 150 MeV/nucleon, producing a 115 MeV/nucleon triton beam. The triton beam will be used in (t,^{3}He) charge-exchange experiments at the S800 spectrometer at the NSCL. At the target of the S800, a triton rate of 5×10^6 particles per second is achieved, for a primary ^{16}O beam of

100 pnA. The (t,^{3}He) reaction using this beam was tested with a ^{24}Mg target. An excitation-energy resolution of 190 ± 15 keV is achieved.

Key words: Radioactive Triton beam, (t,^{3}He) charge-exchange reaction

PACS: 24.30.Cz, 25.40.Kv, 25.60.-r, 27.20.+n

1 Introduction

Charge-exchange (CE) reactions are widely used to study the spin-isospin response of nuclei [1–3]. A variety of probes are available which can be categorized as either being of the $\Delta T_z = -1$ type, such as the (p,n) or (^{3}He,t) reactions, or of the $\Delta T_z = +1$ type, such as the (n,p), (d,^{2}He) or (t,^{3}He) reactions. One of the main motivations for performing CE experiments is the extraction of Gamow-Teller strengths that are important for estimating weak transition rates (electron capture and β-decay) used in the description of pre-supernovae stars [4]. In addition, CE experiments are used to study isovector giant resonances, and their properties can be related to quantities such as the symmetry energy [5] and the neutron-skin thickness [6]. CE reactions also play a vital role in furthering our understanding of (neutrinoless) double-β decay (see e.g. Ref. [7]).

* Corresponding Author: zegers@nscl.msu.edu

[1] We thank the NSCL cyclotron staff for their efforts during the experiment. This work was supported by the US-NSF (PHY0216783 (JINA) and PHY0110253).

[2] Present address: Department of Physics, University of Michigan, Ann Arbor, MI 48109-1040, USA

[3] Present address: Physics Department, University of Guelph, Ontario N1G 2W1 Canada

Of the above-mentioned probes, the (t,^{3}He) reaction, especially at energies of relevance for the astrophysical studies ($E_t \gtrsim 100$ MeV/nucleon) has been employed the least extensively. Recently, the (t,^{3}He) reaction was studied on ^{12}C, ^{26}Mg and ^{58}Ni targets [8,9] and it was shown that this probe is a valuable addition to (n,p) (see. e.g. Refs. [10,11]) and (d,^{2}He) (see e.g. Refs. [12,13]) reactions for extracting Gamow-Teller strength distributions. These (t,^{3}He) experiments were performed at the NSCL, using a secondary triton beam [4] of 115 MeV/nucleon, produced from a primary ^{4}He-beam of 140 MeV/nucleon [14]. Energy resolutions varied from 200 keV to 300 keV (Full-Width at Half Maximum (FWHM)). Besides the data taken on the above-mentioned nuclei, data were also taken on a series of lighter nuclei [15–17] in earlier studies.

The triton-beam intensities achieved with the primary α beam were $\sim 1 \times 10^6$ pps. To improve the efficiency of (t,^{3}He) experiments, a higher intensity is desirable. In addition, a significant amount of overhead time is now involved in producing a primary α beam since the NSCL K1200 cyclotron has to be operated in stand-alone mode, instead of the usual K500$\bigoplus$K1200 coupled operation [25].

It was, therefore, decided to study an alternative way to produce a secondary triton beam and to improve the triton-beam intensity. This study, involving primary beams of ^{16}O (150 MeV/nucleon) and ^{18}O (120 MeV/nucleon), is the subject of this paper. These are the lightest available beams that can

[4] (t,^{3}He) experiments with primary triton beams have been performed at lower energies: $E_t = 5.7 - 7.8$ MeV/nucleon at the Los Alamos Van de Graaff accelerator [18–20], $E_t \approx 12$ MeV/nucleon at the Daresbury Tandem Van de Graaff accelerator [21,22] and $E_t = 40$ MeV/nucleon at the Kernfysisch Versneller Instituut in Groningen [23,24].

be accelerated in coupled-cyclotron operation. Since ^{18}O is more neutron-rich than ^{16}O, a higher triton yield was expected, but since the goal is to reach triton energies in excess of 100 MeV/nucleon, the higher ^{16}O beam energy could be advantageous. Hence a comparison of these two beams was made.

Besides the limitations set by the primary beam energies and intensities, the energy of the secondary triton beam is further restricted by the capability to transport the tritons from the production point to the the S800 magnetic spectrometer [26]. Depending on the ion-optical tune, the maximum magnetic rigidity ($B\rho$) achievable in the transfer lines ranges from 4.8-5.0 Tm, corresponding to triton energies of 115-125 MeV/nucleon.

In order to obtain high-resolution (t,^{3}He) data, such experiments must be performed in dispersion-matched mode of operation of the beam lines and spectrometer. This limits the momentum spread of the triton beam to $dp/p_0 = 5 \times 10^{-3}$ [26], where p_0 is the central beam momentum and dp the full momentum spread.

2 Experiments

Three test experiments were carried out to determine the optimal mode of operation for producing a secondary triton beam. In the first experiment, the triton production-rates using a primary ^{18}O beam with an energy of 120 MeV/nucleon were determined. In the second experiment, a similar study was performed for a primary ^{16}O beam with an energy of 150 MeV/nucleon. In the third experiment, the details of the triton production with the latter primary beam were further investigated. Finally, the resolution obtainable for

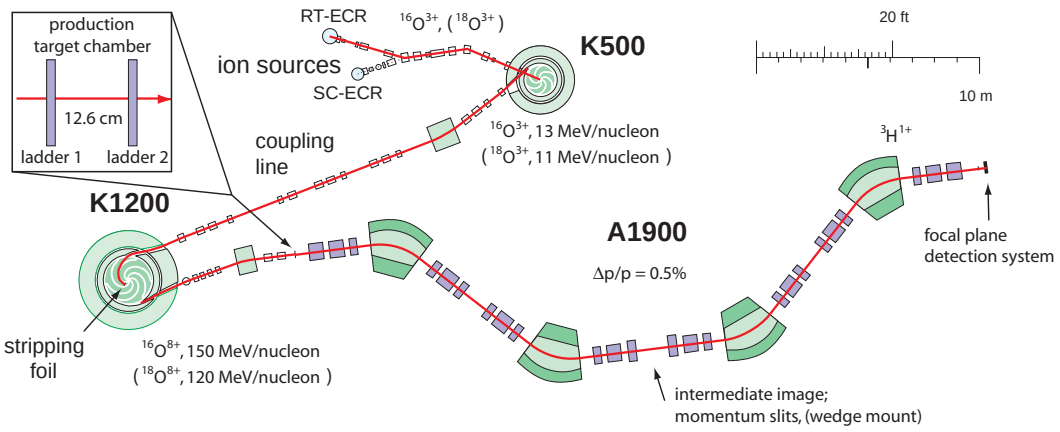

Fig. 1. Schematic view of the NSCL CCF and A1900 fragment separator used in the triton production experiments with ^{16}O and ^{18}O primary beams. The location of the Be production target, the intermediate image with momentum-defining slits, and the focal-plane, where the detectors used to measure the triton rates were placed, are indicated. The inset shows the layout of the production target box with two target ladders.

the (t,^{3}He) reaction at the S800 magnetic spectrometer was studied using a ^{24}Mg target.

2.1 Triton production with a primary ^{18}O beam

A 120 MeV/nucleon $^{18}O^{8+}$ beam produced in the NSCL CCF bombarded a Be production target placed at the entrance of the A1900 fragment separator [27]. The experimental layout is shown in Fig. 1. Three production targets (mounted in ladder 1, see inset of Fig. 1; this position of this ladder corresponds to the nominal A1900 target position) with thicknesses of 1170 mg/cm^2, 2609 mg/cm^2 and 2938 mg/cm^2 were used. Triton yields at magnetic rigidities of 4 Tm and 5 Tm (corresponding to triton energies of 82 MeV/nucleon and 125 MeV/nucleon, respectively) were measured, so that a rough dependence of yield on triton energy could be investigated. The momentum acceptance

was limited to $dp/p_0 = 5 \times 10^{-3}$ by placing a slit at the intermediate image of the A1900.

The secondary particles were detected in the focal-plane of the A1900 and identified by measuring the time-of-flight (TOF) relative to the radio-frequency signal (RF) of the cyclotron and the energy losses in a 100-mm thick plastic scintillator and a 0.5-mm thick silicon PIN detector. In Fig. 2 one sees that the tritons are cleanly separated from other particles produced in the production target. This plot is representative of all measurements presented in this paper, although the relative contribution from contaminants increased at lower magnetic rigidities. For $E_t \geq 110$ MeV/nucleon, it was found that tritons dominate the production yield ($\geq 85\%$). This fraction could be improved by introducing a wedge at the intermediate image of the A1900 to separate particles based on the difference in energy loss. However, events at the S800 that involve beam contaminants and lead to ^{3}He background events are rare and easily removed by means of a TOF measurement. Since the introduction of a 450 mg/cm^2 Aluminum wedge resulted in a small loss in triton yield ($\sim 5\%$), it was decided not to use it in further data taking.

Triton production rates for the various choices of production-target thickness and magnetic rigidity of the A1900 were determined in 5-minute long production runs. The ^{18}O beam intensity was measured at the beginning and end of each run by inserting a Faraday cup into the path of the beam just before the production target. To reduce systematic errors in the extracted triton yields due to fluctuations of the primary beam intensity during a run, the event rate at the focal plane of the A1900 was monitored. The first and last few seconds of each run were used as calibration points for the Faraday-cup measurements. Fluctuations in the event rate at the focal plane were then used to correct for

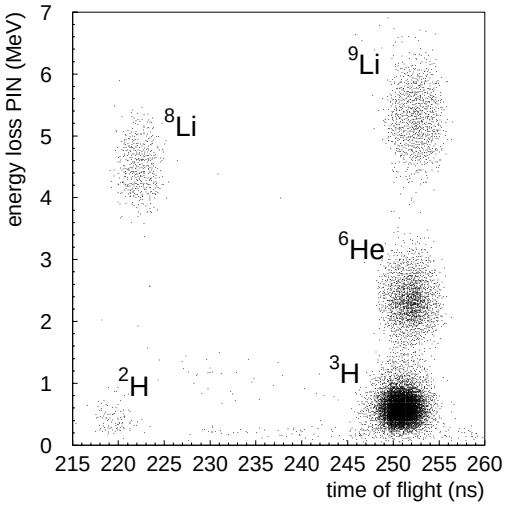

Fig. 2. Typical particle identification spectrum measured in the focal plane of the A1900 during the triton production experiments: the energy loss in PIN detector is plotted versus TOF. The different species can be clearly separated.

fluctuations in the primary beam intensity. In addition to statistical uncertainties, systematic uncertainties in the extracted rates were assigned based on differences between the normalizations using the first and last few seconds of each run.

In Fig. 3, the results for the triton production rates with the ^{18}O beam are presented. A maximum intensity of 7.9×10^4/pnA·s (i.e. per particle nano-Ampère of the primary beam per second) was achieved using the 2938-mg/cm^2 thick Be production target and selecting tritons with an energy of 82 MeV/nucleon. The highest rate achieved at the triton energy of 125 MeV/nucleon is 5.0×10^4/pnA·s. The reduction in triton rate at the higher triton energy is due to the fact that the energy per nucleon of the triton beam is slightly larger than that of the ^{18}O primary beam, and the tail of the distribution has been reached.

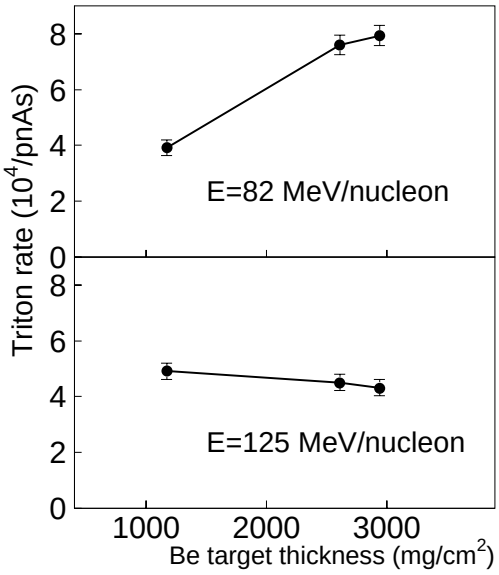

Fig. 3. Triton production rate using an ^{18}O primary beam as a function of production target thickness for triton energies of 82 MeV/nucleon (top) and 125 MeV/nucleon (bottom). The lines are to guide the eye.

2.2 Tritons from ^{16}O, part I

Triton-production rates using a 150 MeV/nucleon primary ^{16}O beam were measured in a similar manner, but with smaller steps in magnetic rigidity (i.e. triton energy). In addition, rates were measured using a wider variety of Be-target thicknesses, ranging from 1480 to 5524 mg/cm^2. By using a combination of targets placed in the two ladders of the A1900 target box (see inset of Fig. 1) steps of approximately 500 mg/cm^2 could conveniently be achieved.

In Fig. 4 the triton production rate as a function of target thickness is shown for different triton beam energies. In Fig. 5, the rates are plotted as a function of triton energy for the different target thicknesses used. In addition to systematic errors arising from the normalization procedures described above (and which are included in the plots), systematic errors arise from the difference in

transmission through the A1900 for tritons generated in the primary production targets located in ladder 1 and ladder 2. By comparing production rates from primary targets of equal thickness in ladder 1 and 2, such uncertainties were determined to be about 5% but depend on the combination of targets used in a particular rate measurement. This systematic error is responsible for the deviations seen from smooth trends in Fig. 4.

Maximum rates ($8 - 10 \times 10^4$/pnA·s) were achieved for triton energies between 116-125 MeV/nucleon ($\sim$80% of the energy per nucleon of the primary beam) using Be target thicknesses between $3 - 4 \times 10^3$ mg/cm^2. At the lowest triton energies, the highest rates are achieved with the thickest Be targets. The optimum target thickness slowly becomes smaller with increasing triton energy.

In comparison to the experiment using ^{18}O at 120 MeV/nucleon as the primary beam, the maximum triton production rate is very similar, but is achieved at a much higher triton energy. For the production of tritons of an energy of 125 MeV/nucleon, the maximum rate achieved with the primary ^{16}O beam at 150 MeV/nucleon is about twice that obtained with the primary ^{18}O beam at 120 MeV/nucleon. For the production of tritons of 82 MeV/nucleon, the results are more or less reversed.

2.3 Tritons from ^{16}O, part II

In the third experiment, the properties of the secondary triton beam produced with a primary ^{16}O beam were further investigated. The goals were to measure the phase-space of the triton beam, the optimum production target

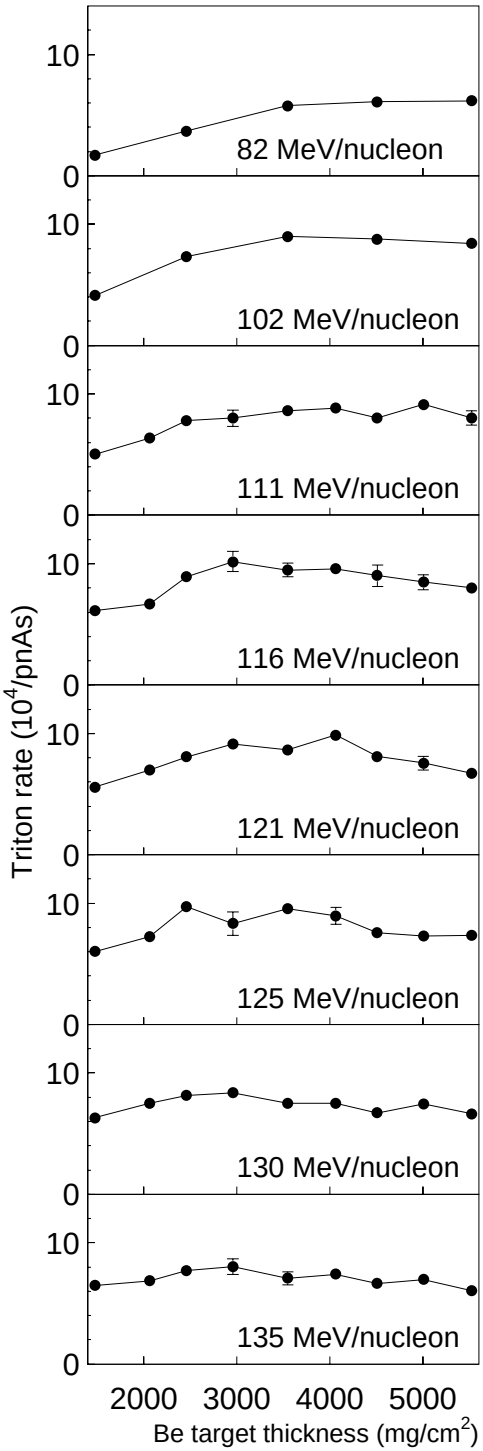

Fig. 4. Triton production rate from fragmentation of a ^{16}O primary beam versus primary target thickness for triton energies as indicated in each panel. For a discussion of systematic errors, see text.

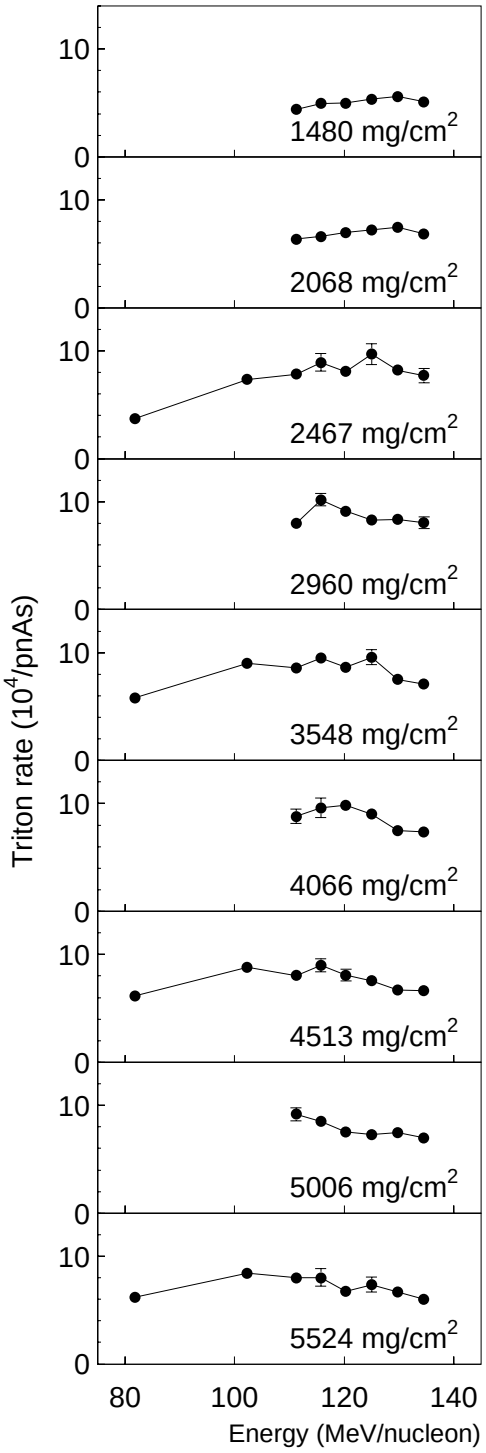

Fig. 5. Triton production rates as a function of triton energy for each of production target thickness used. The thickness of the natural Be target is noted in the lower, right-hand corner of each plot.

configuration and the transmission to the target position in front of the S800 spectrometer.

The phase-space distribution of the triton beam at the focal plane of the A1900 was measured using a pair of parallel-plate avalanche counters (PPACs) [27]. Horizontal (dispersive) and vertical (non-dispersive) positions (x, y, respectively) and angles (θ, ϕ) of the tracks were determined on an event-by-event basis. Data were taken with 1480 mg/cm^2-thick Be production targets in target ladder 1 (see insert, top-left Fig.1), or in target ladder 2, or in both (referred to as "dual-target"). In the dual-target configuration, the phase-space plots (see Fig. 6a for the $x - \theta$-direction) showed two components. By comparing this result with the measurements employing production targets in either ladder 1 (Fig. 6b) or ladder 2 (Fig. 6c) it became clear that one of the components was due to tritons produced at ladder 1 (nominal target position of the A1900) and the other at ladder 2 (not placed at a focus position). To make sure that this effect was a feature arising in normal operation of the A1900, the phase-space distributions were simulated using the Monte-Carlo code MOCADI [28]. The results of the simulation are shown in Fig. 6d-f, and a good correspondence with the experimental phase-space distributions is found. Since it is not possible to achieve optimum dispersion-matching conditions at the S800 spectrometer if the beam consists of two components with different phase-space distributions, it is clear that operation with a single production target is essential.

Since the triton beam produced at the A1900 fills a relatively large phase space, the transmission to the S800 target location is limited by the inner dimensions of the beam-line magnets and transmission lines. To study the transmission of the secondary triton beam, two retractable 1-mm thick in-

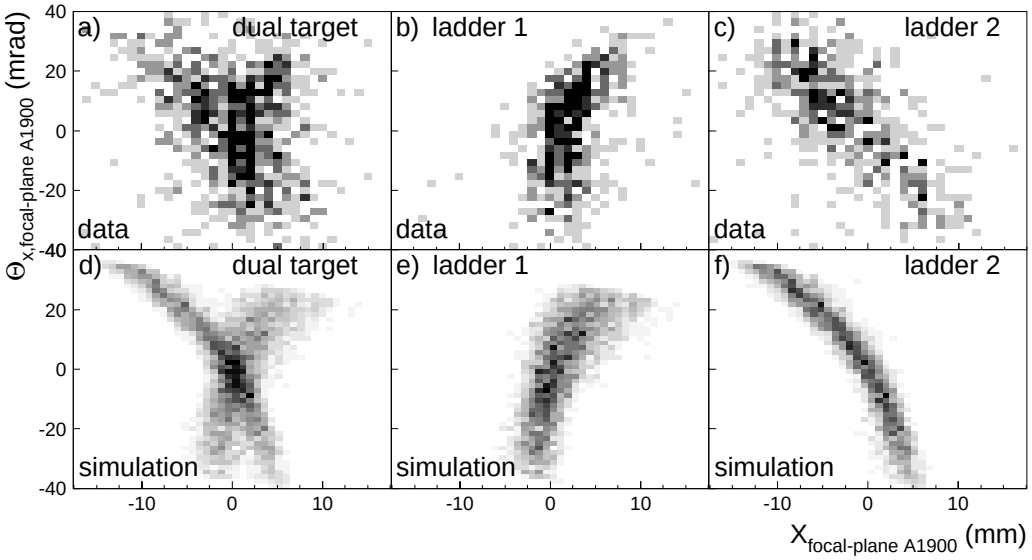

Fig. 6. Phase-space distribution of the secondary triton beam in the horizontal (dispersive) direction in the A1900 focal plane using a) a dual primary-target configuration, b) using a single primary target in ladder 1 and c) using a single primary target in ladder 2. d),e) and f): simulated phase-space distributions using the Monte-Carlo code MOCADI [28] with the same target configurations as in a),b) and c), respectively.

beam scintillators (IBSs) were installed, one at the object of the S800 analysis line (30 m upstream from the S800 target position), the other at the target position of the S800. This transmission study was performed at relatively low triton-beam intensity ($\sim 10^5$ pps) to ensure that efficiencies for detection of the tritons in the IBSs exceeded 95%. The optimal transmissions from the A1900 focal plane to the object in the analysis line and from the object to the S800 target position were $\sim 60\%$ and $\sim 85\%$, respectively, resulting in a total transmission of $\sim 51\%$.

The optimal transmission was achieved at a triton-beam energy of 115 MeV/nucleon ($B\rho$ = 4.8 Tm). At higher energies the current in some of the beam-line magnets could not be increased sufficiently to obtain optimal conditions for

dispersion matching and led to a lower transmission. In light of the phase-space study discussed above, further experiments were performed using a single 3526-mg/cm^2 thick production target in ladder 1 to produce a 115 MeV/nucleon triton beam with an intensity of 4.8×10^4/pnA·s at the S800 target (i.e. including transmission efficiency). Since the primary ^{16}O beam can be accelerated with an intensity of 100 pnA or higher, triton beam intensities of $\gtrsim 5 \times 10^6$ pps can be achieved.

2.4 The ^{24}Mg(t,^{3}He) reaction

The resolution obtainable with (t,^{3}He) reaction with the secondary triton beam was studied by measuring the ^{24}Mg(t,^{3}He) reaction. A 9.86-mg/cm^2 thick, 99.92% isotopically-enriched ^{24}Mg target was used with a triton-beam intensity of approximately 4×10^6 pps. ^{3}He particles were detected in the focal-plane detector system of the S800 [29], consisting of two two-dimensional cathode-readout drift chambers (CRDCs) placed in front of two scintillators. The CRDCs were used to determine the positions and the angles in the dispersive and non-dispersive directions. The first scintillator served as the event trigger and the start of the TOF measurement. The TOF stop signal was given by the cyclotron RF. ^{3}He particles were identified by combining the TOF and $\Delta E - E$ response in the two scintillators. The ion-optical code COSY Infinity [30] was used to calculate the ion-optical transfer matrix of the S800 spectrometer [31] from the measured magnetic field maps. Matrix elements up to fifth order were used in the reconstruction of $\delta = (E - E_0)/E_0$; E_0 is the kinetic energy of the particle following the central-ray trajectory through the spectrometer and E the energy of the measured particle. The track angles

were also obtained in the ray-tracing procedure and used to calculate the ^{3}He scattering angle. From these reconstructed parameters, the excitation energy in ^{24}Na was obtained from a missing-mass calculation.

In Fig. 7a-c the measured excitation energy spectra of ^{24}Na are shown for three different ranges in ^{3}He scattering angle. Fig. 7a shows the spectrum for $\theta_{lab}(^3\mathrm{He}) = 0^\circ - 4^\circ$. A large number of states with varying spin-parity (J^π) are known to reside in the excitation-energy range shown in the figures [12,32]; these are not all resolved. However, Gamow-Teller transitions from the ^{24}Mg $J^\pi = 0^+$ ground state to $J^\pi = 1^+$ states in ^{24}Na are associated with differential cross sections that peak at 0° and thus dominate the spectrum in Fig. 7b ($\theta_{lab}(^3\mathrm{He}) = 0^\circ - 1^\circ$). The state at $E_x(^{24}\mathrm{Na})$=1.35 MeV is predominantly of this type, although it contains $J^\pi = 2^+$ and $3^{(+)}$ components as well (both located at 1.34 MeV [32]). Several, presently unresolved, 1^+ states are known around $E_x(^{24}\mathrm{Na})$= 3.5 MeV [12,32]. Hence the relatively strong peak observed in Fig. 7a. Dipole transitions (angular-momentum transfer $\Delta L = 1$, spin-transfer $\Delta S = 0, 1$) are associated with angular distributions that peak near 3° and transitions with higher angular momentum transfer have rather flat angular distributions at forward angles (see e.g. [8] for the case of ^{26}Mg(t,^{3}He)). Therefore, in Fig. 7c ($\theta_{lab}(^3\mathrm{He}) = 2^\circ - 3^\circ$), transitions to states with $J^\pi = 0^-, 1^-, 2^-, 2^+, 3^+$ become more prominent relative to transitions to 1^+ states. They appear at many excitation energies, but clear examples are seen at $E_x(^{24}\mathrm{Na})$=4.2 and 6.5 MeV.

The excitation-energy resolution at forward scattering angles was determined to be 190 ± 15 keV (FWHM) for the peak at 1.35 MeV in Fig. 7b. Due to the kinematic correlation between ^{3}He angle and energy associated with the recoil of the ^{24}Na residual, and the finite resolution of the ^{3}He angle measure-

ment, the resolution slightly worsens with increasing scattering angle. When integrating over ^{3}He scattering angles between 0° and 4° the energy resolution was 220 ± 10 keV (Fig. 7a). The angular resolution was 0.5° (FWHM), measured using the H(t,^{3}He)n reaction (using a CH_2 target) for which the kinematic correlation between ^{3}He angle and energy is strong.

Part of the energy spread is due to the difference in energy loss of the triton and ^{3}He in the target (50 and 210 keV loss over the full thickness of the ^{24}Mg target, respectively). The energy straggling in the target contributes $\sim 25 - 50$ keV, depending on the location where the (t,^{3}He) reaction takes place in target . Using a simple folding procedure, it was determined that the intrinsic energy resolution (i.e. not related to energy-loss and straggling effects) was 170 ± 15 keV. Under 'optimal' circumstances (object size of 0.5 mm), the energy resolution of the S800 is 1 part in 10000 [26], corresponding to ~ 35 keV for (t,^{3}He) experiments at 115 MeV/nucleon. From the ratio of optimal and deduced experimental resolutions and the known energy dispersion of the S800 spectrometer [5 cm/%($\frac{\delta E}{E_0}$)], it is concluded that the incoherent object size of the secondary triton beam was about 2.5 mm during the experiment. This size is consistent with the size of the beam spot observed using a viewer at the object.

3 Conclusion

We have shown that a high-quality secondary triton beam [E(^{3}H)=115 MeV/nucleon] can be obtained from a 150 MeV/nucleon ^{16}O primary beam. A triton-beam intensity of 9.5×10^4/pnA·s at the focal plane of the A1900 mass separator was achieved with an energy spread of 1%. The transmission of the triton beam to

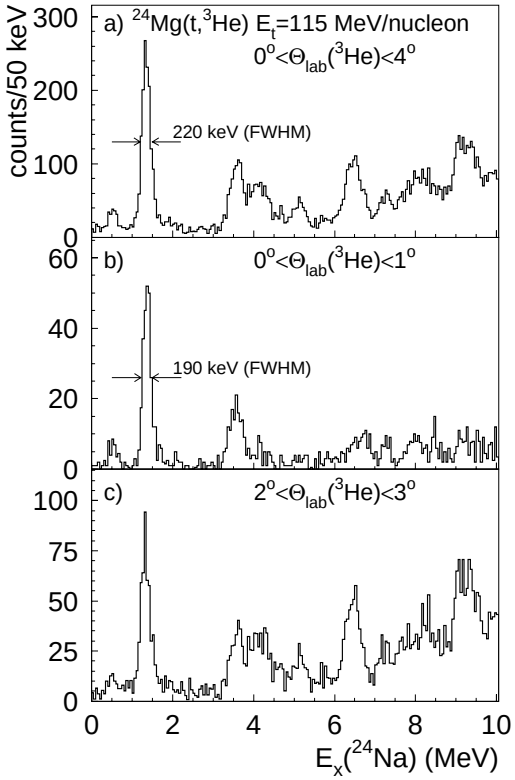

Fig. 7. ^{24}Mg(t,^{3}He) excitation-energy spectra for ^{3}He angular ranges of a) 0°-4°, b) 0°-1° and c) 2°-3° using a secondary triton beam of 115 MeV/nucleon produced with a primary ^{16}O beam of 150 MeV/nucleon. For details, see text.

the S800 target position was 51%. With primary ^{16}O beam intensities available in excess of 100 pnA at the NSCL, triton beam intensities of $\geq 5 \times 10^6$ can be achieved. The ^{24}Mg(t,^{3}He) was studied and an excitation-energy resolution in ^{24}Na of 190 ± 15 keV (FWHM) was achieved at forward scattering angles. The ^{3}He angular resolution was $\sim 0.5°$.

References

[1] F. Osterfeld, Rev. Mod. Phys. **64**, 2 (1992).

[2] M.N. Harakeh and A. van der Woude, Giant Resonances: Fundamental High Frequency Modes of Nuclear Excitations (Oxford University Press, New York,

2001).

[3] T.D. Tadeucci *et al.*, Nucl. Phys. **A469**, 125 (1987).

[4] K. Langanke and G. Martínez-Pinedo, Rev. Mod. Phys. **75**, 819 (2003), and references therein.

[5] P. Danielewicz, Nucl. Phys. **A727**, 233, (2003).

[6] A. Krasznahorkay *et al.*, Phys. Rev. Lett. **82**, 3216 (1999).

[7] H. Ejiri, J. Phys. Soc. Jpn. **74**, 2101, (2005), and references therein.

[8] R.G.T. Zegers *et al.*, nucl-ex/051205 and to be published.

[9] A.L. Cole *et al.*, nucl-ex/0603019 and to be published.

[10] K.P. Jackson *et al.*, Phys. Lett. **B201**, 25 (1988).

[11] W.P. Alford *et al.*, Phys. Lett. **B179**, 20 (1986).

[12] S. Rakers *et al.*, Nucl. Instrum. Methods. Phys. Res. A **369**, 120 (1996).

[13] E.W. Grewe *et al.*, Phys. Rev. C **69**, 064325 (2004).

[14] B.M. Sherrill *et al.*, Nucl. Instrum. Methods Phys. Res. A **432**, 299 (1999).

[15] I. Daito *et al.*, Nucl. Instrum. Methods Phys. Res. A **397**, 465 (1997).

[16] I. Daito *et al.*, Phys. Lett. **B418**, 27 (1998).

[17] T. Nakamura *et al.*, Phys. Lett. **B493**, 209 (2000).

[18] E.R. Flynn, J. Sherman and N. Stein, Phys. Rev. Lett **32**, 846 (1974).

[19] E.R. Flynn, J.W. Sunier, F. Ajzenberg-Selove, Phys. Rev. C **15**, 879 (1977).

[20] F. Azjenberg-Selove, R.E. Brown, E.R. Flynn, J.W. Sunier, Phys. Rev. C **32**, 756 (1985).

[21] K.I. Pearce *et al.*, Phys. Rev. C **35**, 1617 (1987).

[22] N.M. Clarke *et al.*, J. Phys. G **14**, 1399 (1988).

[23] S. Brandenburg *et al.*, Proc. 16^th Int. Conf. on Cyclotrons and their Applications, East Lansing, USA, 13-17 May 2001; AIP Conf. Proc. **600**, 463 (2001).

[24] J. Guillot *et al.*, Phys. Rev. C **73**, 014616 (2006).

[25] The K500⊗K1200, A Coupled Cyclotron Facility at the National Superconducting Cyclotron Laboratory, NSCL Report MSUCL-939, July 1994, unpublished.

[26] D. Bazin, J. A. Caggiano, B. M. Sherrill, J. Yurkon and A. Zeller, Nucl. Instr. Methods Phys. Res. B **204**, 629 (2003).

[27] D.J. Morrissey, B.M. Sherrill, M. Steiner, A. Stolz, I. Wiedenhoever, Nucl. Instr. and Meth. B **204**, 90 (2003).

[28] N. Iwasa, H. Geissel, G. Münzenberg, C. Scheidenberger, Th. Schwab and H. Wollnik, Nucl. Instr. and Meth. B **126**, 284 (1997).

[29] J. Yurkon, D. Bazin, W. Benenson, D.J. Morrissey, B.M. Sherrill, D. Swan, R. Swanson, Nucl. Instr. and Meth. A **422**, 291 (1999).

[30] K. Makino and M. Berz, Nucl. Instrum. Methods Phys. Res. A **427**, 338 (1999).

[31] M. Berz and K. Joh, J. A. Nolen, B. M. Sherrill, A. F. Zeller, Phys. Rev. C **47**, 537 (1993).

[32] P.M. Endt, J. Blachot, R.B. Firestone and J. Zipkin, Nucl. Phys. **A633**, 1 (1998).